Electrochimica Acta 425 (2022) 140708

Contents lists available at ScienceDirect

Electrochimica Acta

journal homepage: www.journals.elsevier.com/electrochimica-acta

An asymmetric MnO_2|activated carbon supercapacitor with highly soluble choline nitrate-based aqueous electrolyte for sub-zero temperatures

Sandra Schrade [a], Zijian Zhao [a,b], Zhazira Supiyeva [b,c], Xinman Chen [d], Sonia Dsoke [a], Qamar Abbas [e,f,*]

[a] Institute for Applied Materials (IAM), Karlsruhe Institute of Technology (KIT), Hermann-von-Helmholtz-Platz 1, Eggenstein-Leopoldshafen D-76344, Germany
[b] Tianjin Key Laboratory of Brine Chemical Engineering and Ecological Utilization of Resources, Tianjin Engineering Center of Marine Chemical Engineering & Technology, College of Chemical Engineering and Materials Science, Tianjin University of Science and Technology, Tianjin 300457, China
[c] Al-Farabi Kazakh National University, 71 al-Farabi Ave., Almaty 050040, Kazakhstan
[d] Guangdong Engineering Technology Research Center of Low Carbon and Advanced Energy Materials, Institute of Semiconductors, South China Normal University, Guangzhou 510631, China
[e] Faculty of Chemical Technology, Institute of Chemistry and Technical Electrochemistry, Poznan University of Technology (PUT), Poznan 60965, Poland
[f] Institute for Chemistry and Technology of Materials, Graz University of Technology (TU Graz), Stremayrgasse 9, Graz 8010, Austria

ARTICLE INFO

Keywords:
MnO_2
CNTs
Choline nitrate
Pseudocapacitance
Low temperature
Supercapacitor

ABSTRACT

MnO_2|activated carbon supercapacitors are attractive power devices that rival the electric double-layer capacitors (EDLCs) due to high reachable voltage. However, they greatly suffer from performance loss at low temperature as most of aqueous electrolytes freeze below ca. -10°C. Here, a concentrated choline nitrate-based (5 mol/L aqueous $ChNO_3$) electrolyte is applied to extend the working temperature range due to its eutectic-like properties. In such electrolyte, water acts as hydrogen bond donor for nitrate anion and low hydration energy for large choline cations favors ionic transport. The MnO_2/CNT composite electrode with a hierarchical structure has been synthesized by hydrothermal process. The presence of CNTs as core component facilitates the electron conduction, while the two-dimensional MnO_2 flakes grown on the surface provide electrolyte transport pathways and improve the interfacial processes (pseudocapacitive charge/discharge). Thanks to the low hydration of choline cation, the individual activated carbon (AC, negative) and MnO_2/CNT (positive) electrodes are charged symmetrically up to a cell voltage of 1.8 V. Overall, due to the wide electrochemical stability window (~2.0 V) and anti-freezing properties of $ChNO_3$-based aqueous electrolyte and the hierarchical design of the MnO_2/CNT composite, the asymmetric supercapacitor operates down to -40 °C and displays excellent energy and coulombic efficiency with no loss of performance after several thousand cycles. This work provides a new possibility on the low temperature application of high voltage supercapacitors.

1. Introduction

Supercapacitors (SCs) are high-power devices that should be able to operate under harsh conditions with minimum risk to the environment. Electric double-layer capacitors (EDLCs) are the commercially available devices that use organic electrolytes with acetonitrile-based hazardous solvents and carbonaceous-based electrodes. EDLCs with organic electrolytes display high cell voltage up to 2.7-2.85 V, however, with risks of fire and hazardous gases under emergency situations [1–4]. Low cost and eco-friendly alternatives to these electrolytes are the aqueous ones with non-flammable and overall sustainable characteristics. A serious drawback with aqueous electrolytes based supercapacitors is the oxidation of positive carbon electrode that limits the voltage window to 1.5 or 1.6 V [5]. One way to counter this issue is the use of concentrated electrolytes where scarcity of free-water prevents from oxidation processes and enables reaching high cell voltages ca. 2.0 V [5,6].

Another strategy that solves the problem of carbon oxidation and enhances the cell voltage is to replace the positive carbon electrode with a MnO_2 pseudocapacitive electrode [7–9]. The oxidation limit of the MnO_2 in aqueous electrolytes is ~1.2 V vs RHE which is much larger than the stability window of carbon electrodes and can result in cell voltages up to 2.0 V or 2.2 V. Nevertheless, at high cell voltage conditions and during long-term cycling, the structure and morphology of MnO_2 are compromised due to the Mn oxidation state changes

* Corresponding author at: Institute for Chemistry and Technology of Materials, Graz University of Technology (TU Graz), Stremayrgasse 9, Graz 8010, Austria.
E-mail address: qamar.abbas@tugraz.at (Q. Abbas).

https://doi.org/10.1016/j.electacta.2022.140708
Received 14 March 2022; Received in revised form 16 May 2022; Accepted 12 June 2022
Available online 13 June 2022

(conversion of Mn^{4+} to Mn^{7+} at high potential) [10]. This voltage push can seriously damage the electrode integrity and deteriorate the device's performance. Indeed, a cell voltage of 1.7–1.8 V is reachable with MnO_2| carbon device where a positive MnO_2 electrode only operates below its oxidation limit. This approach prevents the positive electrode from oxidation and makes it easy to achieve a long cycle life and a higher energy density than that of symmetric carbon/carbon supercapacitors.

An important aspect of MnO_2|carbon supercapacitor in aqueous neutral electrolytes (pH ~ 7.0) is the overpotentials at both positive and negative electrodes that lead to a high cell voltage. In other words, the positive MnO_2 possesses the overpotential for aqueous electrolyte oxidation and the negative porous carbon electrode shows a high overpotential for hydrogen evolution [11]. Hence, two electrochemical phenomena combined in a single cell make this family of SCs an attractive high energy storage option. Carbon nanotubes (CNTs) have been often used to stabilize MnO_2 and to increase the conductivity of pseudocapacitive materials, and these nanocomposite materials have been the subject of extensive research in the supercapacitor field [12–14]. CNTs enable enhanced surface accessibility of MnO_2, improve the bulk electrode conductivity as well as facilitate the ionic movement by providing facile pathways for the electrolyte.

The charging mechanism of MnO_2 has been widely discussed in recent years [15–17] with a broad agreement on its pseudocapacitive behavior. However, the charge compensation for the Mn^{4+}/Mn^{3+} valence state variation has been dedicated to alkali cations or H^+ ions in acidic medium. In the case of bulky anions and cations [18], such as in 1-Ethyl-3-methylimidazolium thiocyanate ionic liquids, anions are found to be responsible for compensating the charge during Mn^{4+}/Mn^{3+} conversion. The use of SCN^- and PF_6^- has shown an influence on the MnO_2 capacitance as well, and therefore, the presence of larger cations with loose ion-pairing could enforce a different charge storage mechanism. It might be that a bulky cation, via better dissociation of ionic species, favors a charging of MnO_2 electrode with anions. Charging of MnO_2 electrode is also dependent on its structural properties: adsorption/desorption mostly occurs on amorphous MnO_2, while insertion/de-insertion takes place in crystalline compounds.

Despite several advantages of aqueous electrolytes, whether used in carbon/carbon symmetric or MnO_2|carbon asymmetric SCs, their freezing at low temperatures limits the scope of application. Water/alcohol-based binary mixtures exhibit low freezing temperature, however, owing to the reduce salt solubility in them, the total quantity of ionic species available for charging the electric double layer (EDL) is insufficient, leading to reduced capacitance. Furthermore, water and alcohols have different affinity for porous carbon electrode that disturbs the local ionic concentration in the bulk electrolyte and in confined nanopores [19]. The electrolyte conductivity is another parameter that is important for achieving high SC power, and aqueous electrolytes often have a serious issue of freezing at low temperatures. On the other hand, high salt concentration is needed for the majority of ions to efficiently penetrate the pores and charge EDL at the negative carbon electrode, or to facilitate the pseudocapacitive charging at the positive MnO_2 electrode. Choline nitrate is highly soluble up to 30 mol/kg of water, and such a high concentration is possible due to the eutectic-like properties of choline salt [20], similar to the ones described for choline chloride/urea or choline chloride/ethylene glycol deep eutectic solvents [21–23]. Previously, using choline salt-based aqueous electrolyte (5 mol/L ChCl), carbon/carbon supercapacitors have shown excellent electrochemical performance down to -40°C [24].

Here, MnO_2/CNT|carbon supercapacitor that operates effectively down to -40°C with a voltage window of 1.8 V has been proposed. The MnO_2/CNT nanocomposite displays improved performance as it facilitates the electrolyte accessibility, enhances the electronic conductivity of the bulk electrode and increases the charge storage characteristics. Then choline nitrate-based neutral aqueous electrolyte (at a selected concentration of 5 mol/L with highest ionic conductivity of 82 mS/cm) enables enhanced voltage at room temperature as well as its eutectic-like characterisitcs with water enables excellent low-temperature performance of the supercapacitor at sub-zero temperatures.

2. Experimental

2.1. Hydrothermal synthesis

All the chemicals and materials used in this study were purchased at high quality from Sigma-Aldrich. The multiwalled CNTs (Sigma Aldrich, CAS-308068-56-6, d x l: 110–170 nm x 5–6 μm) were added to 10 wt.% HNO_3 and stirred at 80 °C for 12 h. Afterwards, the treated CNTs were filtrated and washed three times with deionized water and finally dried at 100 °C overnight and for 12 h at 120 °C in a vacuum. The MnO_2/CNT nanocomposite was prepared according to the procedure proposed by Xia et al. [25], where 100 mg of acid-treated CNTs were mixed with 70 ml of water under ultrasonic conditions (in a P120H Ultrasonic bath from *ELMASONIC*). This step was followed by the addition of 0.3 g of $KMnO_4$ to the mixture under stirring for 2 h. The mixture was transferred to teflon-lined, stainless steel autoclave where the treatment was carried out at 150°C for 6 h. After careful removal of the prepared MnO_2/CNTs nanocomposite, it was filtered and washed with deionized water and dried at 80°C for 48 h. The MnO_2 was prepared as a control sample. 0.3 g of $KMnO_4$ and 1.5 ml HCl (37 wt.%) was dissolved in 70 ml water to form a mixture. Then the mixture was transferred to the autoclave and heated at 150°C for 4 h. The obtained two samples were black powder, which were then transferred for characterization with different techniques.

2.2. Physicochemical characterization

The morphology of the MnO_2/CNT nanocomposite was investigated with scanning electron microscopy (Zeiss Supra 55 Scanning Electron Microscope (SEM) with primary energy of 15 keV) and the structural information of MnO_2, CNTs and MnO_2/CNTs with Raman spectroscopy at a laser wavelength of 645 nm by using. Raman measurements were performed by a Raman spectrometer (LabRam Evolution HR, Horiba Jobin Yvon) using 532 nm laser excitation with a power of 10 mW. X-ray powder diffraction (XRD) was carried out with a STOE Stadi P XRD diffractometer (50 kV, 40 mA) in Debye–Scherrer geometry with Mo Kα1 radiation ($\lambda = 0.70932$ Å). Thermogravimetric analysis (TGA) was realized through a thermogravimetric analyzer (STA 449C, Netzsch GmbH) under Ar/O_2 flow (30/10 ml min^{-1}) from 30 to 800°C with a heating rate of 10°C min^{-1}.

2.3. Electrolyte and electrodes

Choline nitrate was prepared by a simple metathesis reaction of choline chloride, where choline hydroxide was derived via reaction with Ag_2O (used as mild oxidizing agent), the precipitated silver chlorie was filtered out, and followed by the addition of HNO_3 to the filtrate until reaching a neutral pH [20,26]. The stability window of 5 mol/L $ChNO_3$ was investigated in a three-electrode beaker setup on a gold working electrode with a large platinum counter electrode and Ag^+/AgCl reference electrode. The potential window was scanned at a rate of 10 mV/s between -1.6 V to +0.7 V.

For the construction of supercapacitors, self-standing pellet electrodes were prepared by mixing 90 wt.% of carbon (YP80F, Kuraray), or 85 wt.% MnO_2/CNT nanocomposite with 5 wt.% poly(tetrafluoroethylene) binder (PTFE - 60 wt.% dispersion in water, Sigma-Aldrich) and 5 or 10 wt.% carbon black (Super C65, Imerys) as conductivity enhancer. The three components for each type of electrode were mixed in ethanol (Sigma-Aldrich, 99.5%) until a dough was obtained. Then the dough was rolled into a homogenous electrode sheet that was dried under vacuum at 110°C for 12 h with a final thickness ~100 μm. The pellets of electrodes with a diameter of 11 mm (8–10 mg of active materials) were punched out to assemble the supercapacitor cells.

2.4. Electrochemical characterization of supercapacitor cells

The electrochemical performance of full supercapacitors was tested in Teflon Swagelok® vessel at all temperatures from -40 °C to + 60 °C in a customized climatic chamber. The electrolyte was prepared from choline nitrate or lithium nitrate at a concentration of 5 mol/L for assembling the supercapacitor cells with current collectors made of stainless steel (type 304), and microfiber filter GF/A (WhatmanTM, thickness = 0.26 mm) was used as a separator, sandwiched between the electrodes. The two-electrode setup equipped with a reference electrode configuration was used to monitor the behaviour of the positive (MnO_2) and negative carbon electrodes in the cell (with an optimal active mass ratio of 1:1). In case of the three-electrode configuration, where a large microporous-carbon based counter electrode (30 times higher active mass than the working electorde) was used, the electrochemical properties of MnO_2 were investigated. In both types of cells, Ag^+/AgCl in 3.0 mol/L KCl was used as reference electrode. The electrochemical performance of the two- and three-electrode cells with reference electrode was determined with a VMP3 (from Biologic) multichannel potentiostat/galvanostat. The gravimetric capacitance C (F g^{-1} of active materials in two electrodes) was estimated from the integration of the galvanostatic discharge curves at 0.5 A g^{-1}. The specific current used for testing is estimated from the total mass of active material in two electrodes.

3. Results and discussion

The physicochemical and electrochemical properties of MnO_2/CNT nanocomposite material were investigated, while keeping in view the stability window of 5 mol/L $ChNO_3$ electrolyte. The charging behavior of MnO_2 and carbon electrodes in 5 mol/L aqueous $ChNO_3$ and $LiNO_3$ electrolytes is discussed. Then, the asymmetric (+)MnO_2/CNT|YP80F(-) supercapacitor in aq. $ChNO_3$ is tested at 24 °C, down to -40 °C and at 60 °C. For high-temperature investigations, another supercapacitor cell with similar configuration was assembled, while room temperature and -40 °C measurements were conducted on the same cell.

3.1. Physicochemical characterization of MnO_2/CNT composite electrode

The MnO_2/CNT composite morphology is characterized and shown in Fig. 1a,b. The elongated MnO_2 crystalline layers are covering the CNTs structure forming a pattern via arrangement on the entire outer surface of nanotubes. The regular oblique layered structures with a diagonal length of approximately 100–150 nm can be seen. An equal distribution of MnO_2 onto the nanocomposite material indicates a homogeneous structure and suggests good connectivity of particles, which is crucial for the electron conductivity. The extended and uniform pillars of MnO_2 can provide a high available surface area, where the excess (reservoir) of electrolyte can be held and can improve the electrode/electrolyte interface.

Fig. 1c shows the Raman spectra of pristine MnO_2, pristine CNTs and MnO_2/CNTs nanocomposite, which are characterized by the respective Raman peaks related with the structural features. Raman peaks for CNTs at 1334 cm^{-1} and 1593 cm^{-1} indicate the well-known D- and G-bands, respectively typical for the carbon material parameters, while the MnO_2 Raman spectra is characterized by a peak at 645 cm^{-1} [25,27]. The MnO_2/CNT nanocomposite maintains the structural characteristics of both CNTs and MnO_2, as shown by the Raman spectrum. The composite material is characterized by broader D- and G-band peaks, which could be due to the interactions between MnO_2 and CNTs and different crystals orientation. The thermograms (Fig. 1d) show a slight mass loss of 4% for MnO_2 and up to 38% of mass loss for MnO_2/CNT nanocomposite. This indicates that the MnO_2 sample is stable until ~600 °C and the higher mass loss of the MnO_2/CNT composite is due to the burning off of the CNTs in the composite. Hence, the total CNTs content in the MnO_2/CNT composite is about 38 wt.%. Fig. 1e shows the XRD patterns of the CNTs, the pure MnO_2, and the MnO_2/CNT nanocomposite. The XRD pattern of the CNTs exhibits diffraction peaks at 12.3°, 19.5° and 34°, which can be

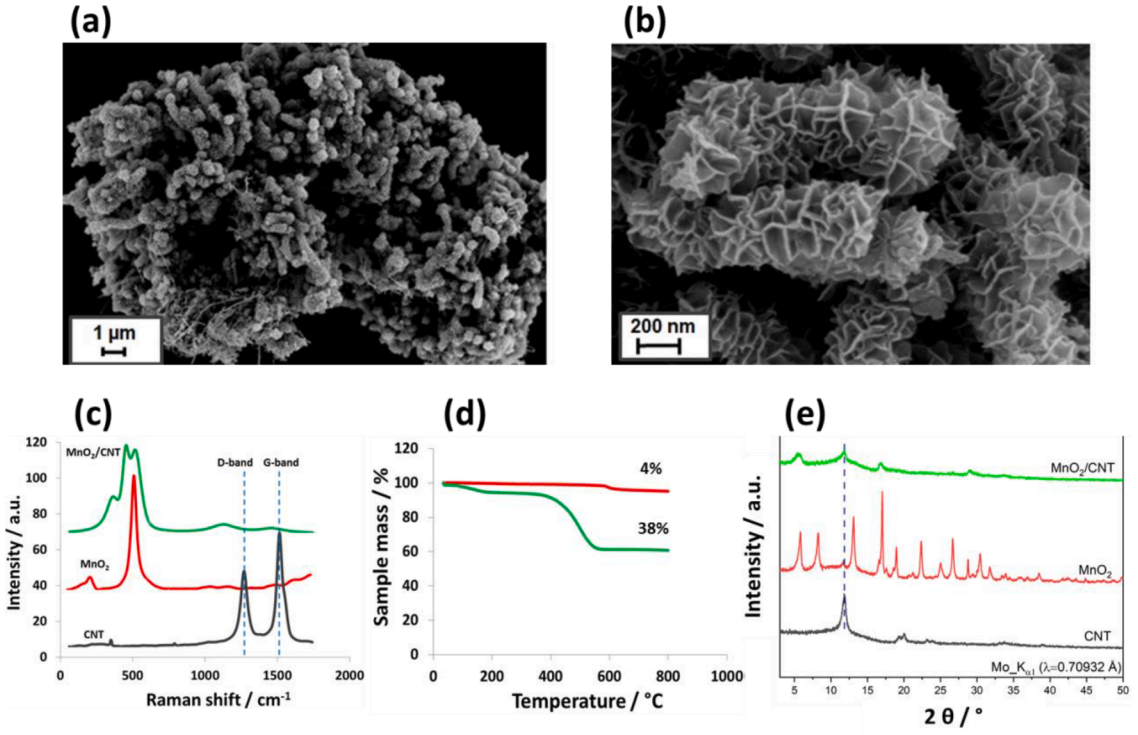

Fig. 1. (a,b) SEM images of MnO_2/CNT nanocomposite material at different magnifications, (c) comparison of Raman spectra for MnO_2/CNT, MnO_2 and CNT realized with a laser wavelength of 532 nm, (d) Thermogravimetric analysis of MnO_2 and MnO_2/CNT up to 800°C in Ar/O_2 flow (30/10 ml min-1), (e) XRD patterns of MnO_2/CNT nanocomposite, pure MnO_2 and CNT with Mo Kα1 radiation (λ = 0.70932 Å).

attributed to the reflections (002), (100) and (004) of graphite [28]. The XRD patterns of the pure MnO_2 powder can be indexed to the tetragonal α-MnO_2 (JCPDS 44-0141) [27]. Regarding the MnO_2/CNT composite, the MnO_2 can be indexed to the monoclinic birnessite type MnO_2 (JCPDS 80-1098) [25], and the diffraction peak from the CNTs at 12.3° can still be observed.

The electrochemical stability windows in Fig. 2a were determined for a 5 mol/L $ChNO_3$ electrolyte on a gold working electrode between a potential range of -1.6 V to 0.7 V vs Ag^+/AgCl (scan rate = 10 mV/s). The potential window is characterized by a flat current versus potential profile between -1.3 to 0.6 V, indicating a stable electrochemical behavior of the electrolyte. The positive scan towards 0.7 V is followed by an oxidation peak, while a strong reduction peak is visible at negative potentials down to -1.3 V. According to the presented scans in Fig. 2a, 5 mol/L $ChNO_3$ is electrochemically stable in the range of -1.2 to 0.6 V vs. Ag^+/AgCl. Fig. 2b, c depicts the ionic species dissociation which is due to the hydrogen bond donor ability of water, similar to the effects observed in formation of deep eutectic solvents [21–23]. We have observed similar depression of freezing point in case of 5 mol/L $ChNO_3$ determined by the differential scanning calorimetry data presented in Fig. 2d.

3.2. Charge storage in aqueous choline nitrate- and lithium nitrate-based electrolytes

The charge storage of MnO_2/CNT compsite and carbon electrodes are investigated in a two-electrode cell using 5 mol/L $LiNO_3$ or $ChNO_3$ with a reference electrode setup. The cell voltage window is scanned up to a limited value of 1.0 V in order to preserve the electrolyte from oxidation and a low specific current of 0.1 A/g is used to make sure a slow electrode charging and a proper wetting of the electrodes. Fig. 3 shows that the positive electrode in aq. $LiNO_3$ displays low capacitance while the positive and negative electrodes in aq. $ChNO_3$ show nearly equal capacitance. In aq. $LiNO_3$ The positive MnO_2 electrode reaches a maximum potential of 0.7 V vs Ag^+/AgCl while the maximum potential is 0.44 V in aq. $ChNO_3$. Thereby, the positive electrode potential range $\Delta E_+ = 0.53$ V and negative electrode potential range $\Delta E_- = 0.14$ V in aq. $LiNO_3$, while the MnO_2/carbon cell with aq. $ChNO_3$ where $\Delta E_+ = 0.32$ V and $\Delta E_- = 0.35$ V (potential distribution is nearly equal between the electrodes.

The disparity of potential range and consequently the capacitance of each electrode in aq. $LiNO_3$ can be explained based on the ionic association between strongly hydrated lithium and the nitrate ions. At higher concentrations, lithium ions tend to form ion pairs and this property of lithium-based electrolytes strongly influence the charging of carbon nanopores [20,29]. On the other hand, a loosely hydrated choline cation is better dissociated in the aqueous electrolyte, which results in better charging of both positive MnO_2 and negative carbon electrodes [20]. It might be that the choline cation owing to its dissociation, allows the nitrate anion to compensate charges for the Mn^{4+}/Mn^{3+} oxidation state changes during charge/discharge. It has been previously reported that cations are the main species in aqueous lithium nitrate electrolytes that compensate for this redox reaction, which could arise from the strong association of lithium with the respective anion. On the other hand, in the case of large cations such as choline, the charging of MnO_2 would be different and controlled mainly by the anions, in this case the NO_3^{-1} ions.

3.2. Electrochemical behavior of MnO_2/CNT electrode

Galvanostatic charge/discharge curves in Fig. 4a (MnO_2|YP80F) and

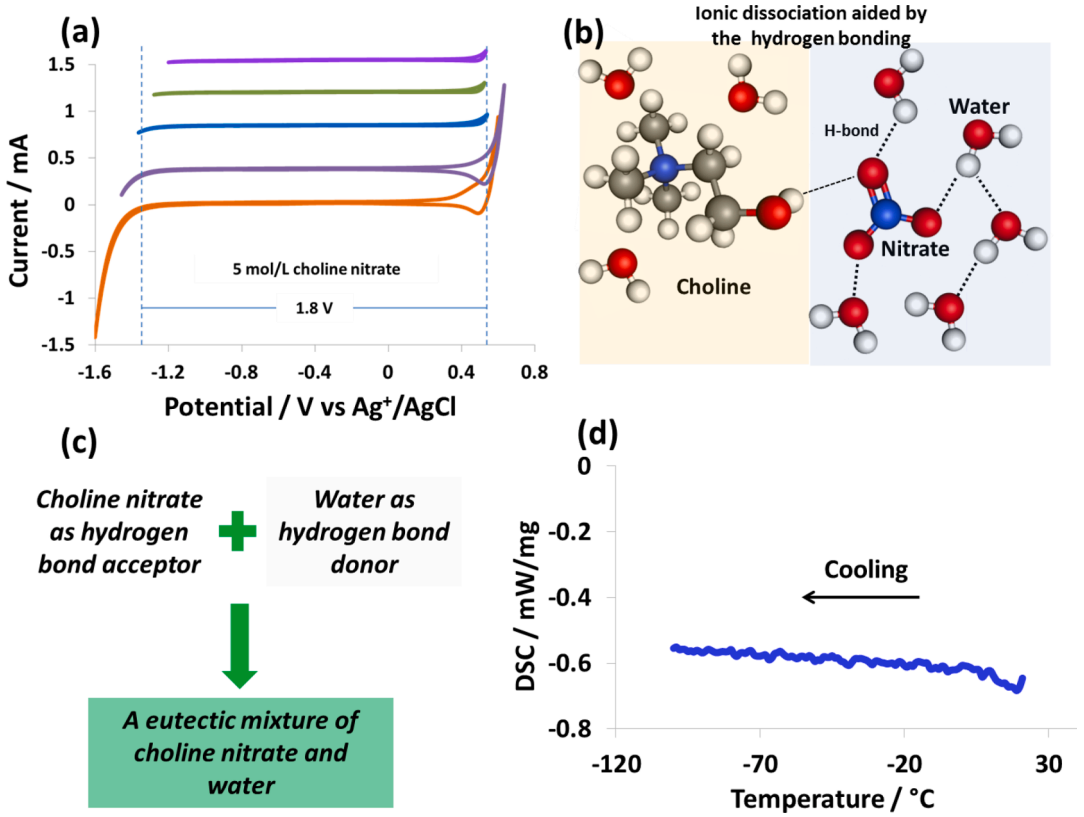

Fig. 2. (a) Electrochemical stability window of 5 mol/L choline nitrate tested with gold (Au) working electrode, platinum (Pt) counter electrode and Ag^+/AgCl in 3 mol/L KCl as a reference electrode in a beaker cell. The potential window was scanned at 10 mV/s from lower values to the higher values with a gradual increase on both positive and negative polarities, (b, c) schemes showing the formation of eutectic mixture between choline nitrate and water (molar ratio of 1:11), where former acts as hydrogen bond acceptor (HBA) and the latter as hydrogen bond donor (HBD), (d) differential scanning claorimetry at 10°C/min shows the absence of any thermal event when cooling down 5 mol/L choline nitrate solution from 25°C to -100°C.

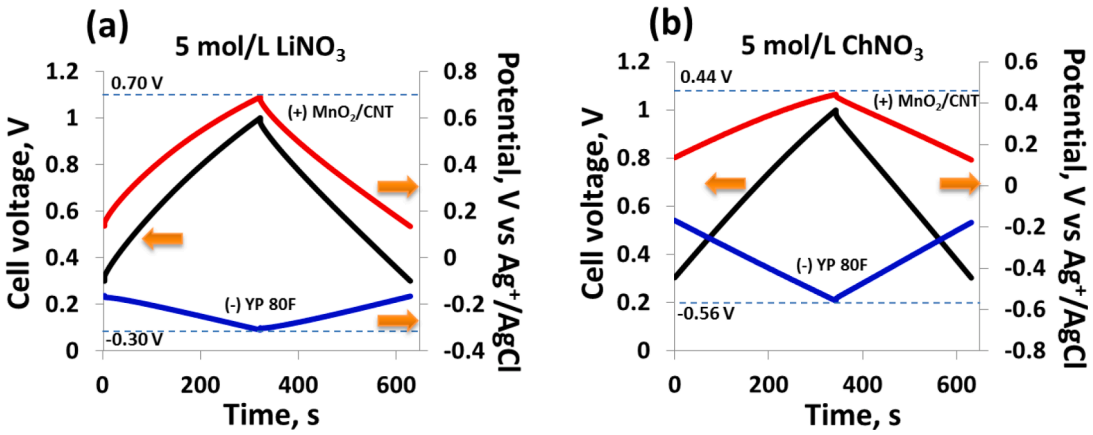

Fig. 3. Galvanostatic charge/discharge testing of MnO_2-CNT|YP80F asymmetric supercapacitor at 0.1 A/g in (a) 5 mol/L $LiNO_3$ and (b) 5 mol/L $ChNO_3$ (choline nitrate) at room temperature in a selected potential window of 0.3 to 1.0 V by using a two-electrode cell configuration with a reference electrode setup. MnO_2/CNT is the positive electrode and YP80F is the negative electrode, Ag^+/AgCl is used as a reference electrode. An equal mass of active materials in two electrodes was selected for these cells.

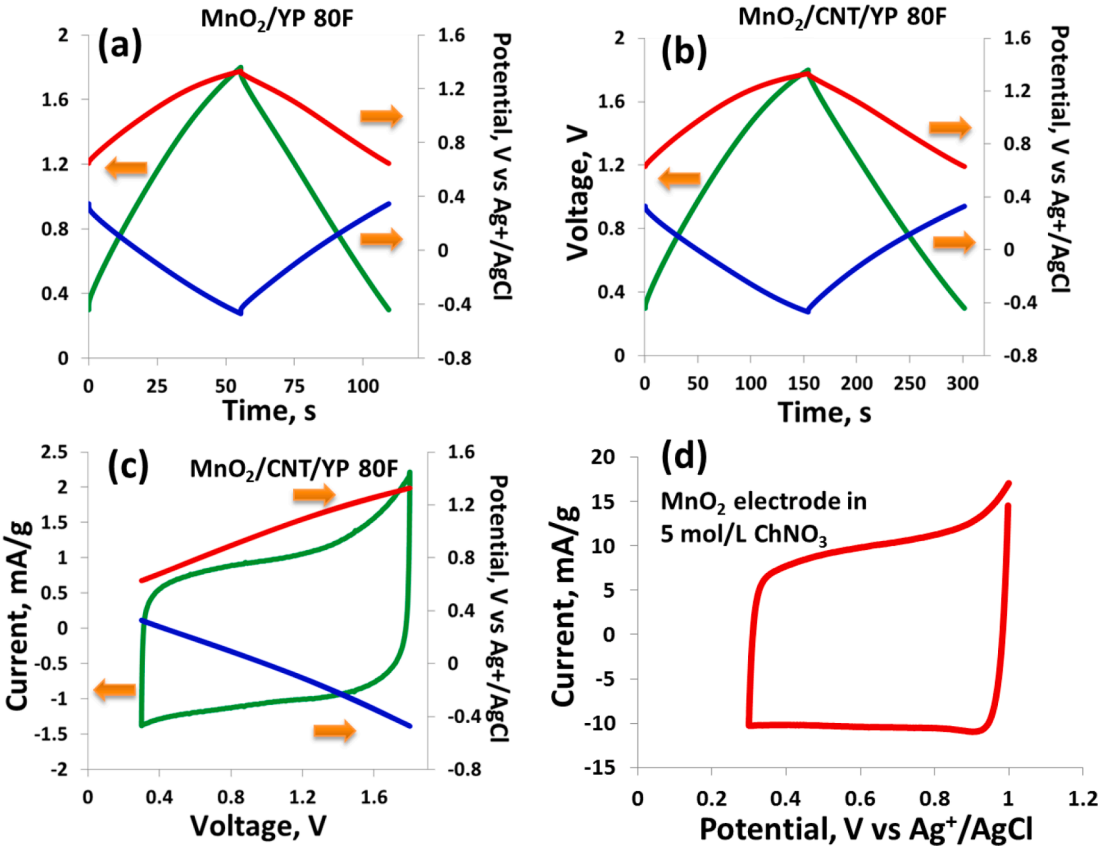

Fig. 4. Galvanostatic charge/discharge testing of (a) MnO_2 and (b) MnO_2/CNT electrodes at 200 mA/g in 5 mol/L choline nitrate at room temperature, (c) cyclic voltammetry of two-electrode with reference where MnO_2/CNT is positive and YP80F is negative electrode, the red and blue lines show the potential excursions (potential ranges) of positive and negative electrodes, respectively (d) cyclic voltammogram of MnO_2/CNT electrode in 5 mol/L choline nitrate in a selected potential window of 0.3 V to 1.0 V by using three-electrode setup where Ag^+/AgCl (in 3 mol/L KCl) is used as reference electrode with large area activated carbon as counter electrode.

Fig. 4b (MnO_2/CNT|YP80F) show the influence of CNTs on the electrochemical behavior of MnO_2 in 5 mol/L $ChNO_3$. At a specific current of 0.2 A/g and a cell voltage up to 1.8 V, the positive MnO_2 electrode (Fig. 4a) shows symmetric charge/discharge curves. Although both positive and negative electrodes in this cell display a triangular shape of curve, the charge storage mechanism is different for the two electrodes. The negative carbon electrode stores charges at the electric double-layer and possesses a high overpotential for the reversible hydrogen adsorption/desorption, which enables reaching high cell voltage [11]. In the case of MnO_2/CNT|YP80F cell (Fig. 4b), the CNTs aids MnO_2 to deliver enhanced pseudocapacitive behavior, which is evident from the higher capacitance (17 F/g for MnO_2 and 41 F/g for MnO_2/CNT-based electrode). Thanks to the better connectivity of MnO_2 crystals, and easy electrolyte accessibility via channels creating improved

MnO_2/electrolyte interface [30], high charge storage is achieved in MnO_2/CNT|YP80F cell as compared to the MnO_2|YP80F cell.

In the charge/discharge curves of Fig. 4a, b, the positive electrode displays a noticeable change in charge/discharge slope at high potentials near 1.2 V vs. Ag^+/AgCl, also indicated by the inceased current at high potential in the CV of Fig. 4c,. This is due to the fact that the MnO_2 electrode reaches the overpotential limit at high potential values, near the oxidation limit of electrode/electrolyte. In this asymmetric cell, the overall charge/discharge characteristics are determined by the pseudocapacitive MnO_2-based electrode. This assumption follows the equation of capacitance for two capacitors connected in series $1/C_{cell} = 1/C_{YP80F} + 1/C_{MnO2}$, where the electrode with lower capacitance (MnO_2-based one) determines the overall cell capacitance. Here, the capacitance differences between the two electrodes are minor, still the charge/discharge pattern of the cell is similar to the positive MnO_2 electrode.

The cyclic voltammogram shown in Fig. 4c up to 1.8 V is characterized by a square-type shape indicating a supercapacitor-like behavior. The low cut-off voltage in this type of asymmetric supercapacitor cells is selected 0.3 V to avoid the positive MnO_2 electrode from operating below a certain potential window. In other words, the MnO_2 electrode is susceptible of operating below 0.2 V vs SHE if the cell is discharged below 0.3 V, leading to the reduction of Mn^{4+} to Mn^{2+} that can severely damage the electrode morphology and integrity [10]. Likewise, the positive MnO_2 electrode should not operate beyond 1.2 V vs. SHE to avoid the oxidation of Mn^{4+} to Mn^{7+}, which can deteriorate the cell performance. Therefore, based on the two-electrode with reference electrode studies, a careful cell potential window is selected between 0.3 V to 1.8 V in this work.

The cyclic voltammogram in Fig. 4d is obtained in a three-electrode setup (half-cell) where MnO_2/CNT electrode stability is demonstrated between 0.3 V to 1.0 V vs. Ag^+/AgCl. Square-shape of the cyclic voltammogram indicates an ideal pseudocapacitive charge storage in 5 mol/L $ChNO_3$. At higher potential, a relative increase of charging current suggests the surface changes related to the oxidation of Mn^{4+}. One of the important aspect of MnO_2/CNT|YP80F asymmetric supercapacitor is the low negative potential reached at the nanoporous carbon electrode, where electrolyte reduction causes hydrogen production, that is partially stored in the nanoporous carbon and partially extracted during repeated oxidation/reduction cycles. Thus, a reversible hydrogen adsorption/desorption in the nanoporous carbon electrode facilitates the enhanced cyclability of the supercapacitor cell. Overall, an optimized balancing of positive and negative electrodes leads to an optimized MnO_2/CNT|YP80F asymmetric supercapacitor in choline nitrate-based aqueous electrolyte.

3.3. MnO_2/CNT|YP80F supercapacitor performance from 24°C to -40°C

Asymmetric MnO_2/CNT|YP80F supercapacitor in 5 mol/L $ChNO_3$ in a two-electrode setup is electrochemically tested between 0.3 V and different cut-off values up to 1.8 V at 24°C and the charge/discharge curves and cyclic voltammograms are presented in Fig. 5. Symmetric charge/discharge curves are obtained at 0.5 A/g and the CVs display square-type shape even at high scan rates, as presented in Fig. 5a and 5b and 5c, respectively. The squared shape of CVs is preserved at 80 mV/s indicating a capacitor-type behavior at high scan rate. Similarly, galvanostatic charge/discharge curves in Fig. 5d are collected at different specific currents (calculated per active mass of two electrodes, at 0.5, 1.0, 2.0 and 4.0 A/g) and even at high specific current, the charge/discharge curves are not only symmetric but display very small ohmic loss. Hence, at high specific current and scan rates, reasonably high capacitance (38 F/g at 1 A/g – specific current calculated per total active mass in two electrodes) can be extracted from the MnO_2/CNT|YP80F supercapacitor.

The MnO_2/CNT|YP80F supercapacitor was cycled galvanostatically for 10000 charge/discharge cycles between 0.3 V and 1.8 V at a specific current of 1.0 A/g. The evolution of capacitance, energy efficiency (calculated from ratio of area under discharge versus charge curve) and coulombic efficiency (calculated from the ratio of discharge time versus charge time) is shown in Fig. 5e. A constant pattern of capacitance (~37 F/g), energy efficiency (~80%) and coulombic efficiency (~90%)

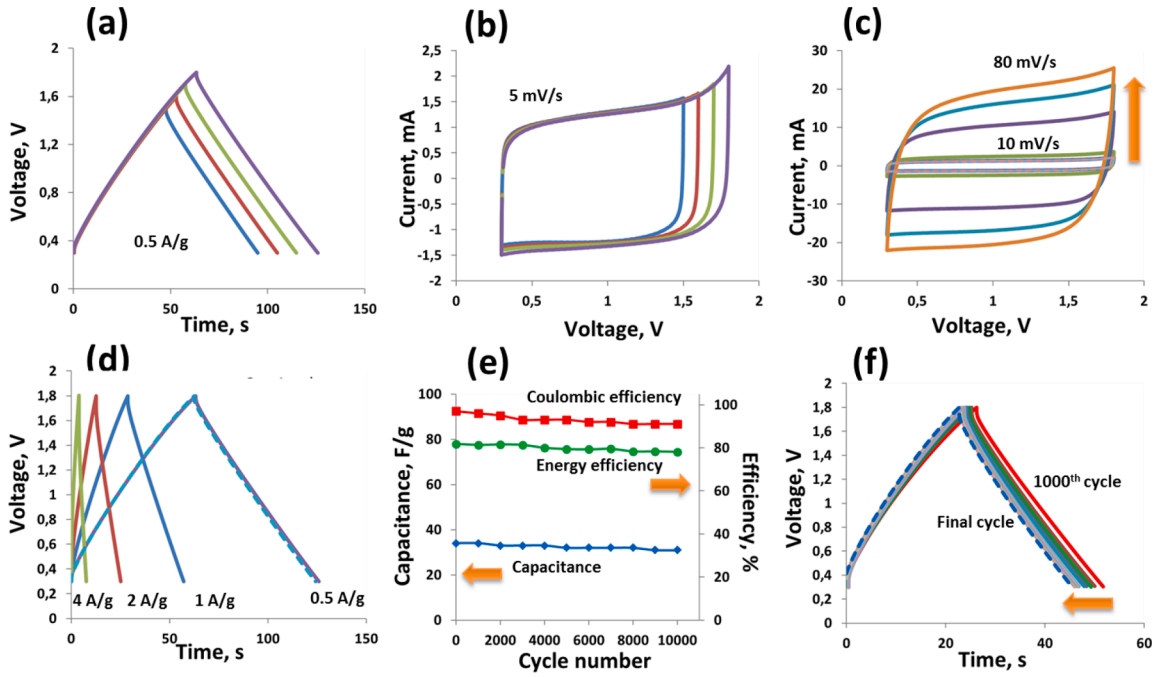

Fig. 5. Electrochemical testing of MnO_2/CNT|YP80F supercapacitor at room temperature and up to 1.8 V, (a) galvanostatic charge/discharge at 0.5 A/g, (b) cyclic voltamogramms at 5 mV/s, (c) cyclic voltammograms at various scan rates from 5 mV/s to 80 mV/s, the arrow shows the direction of increasing scan rate, (d) galvanostatic charge/discharge curves at various specific currents from 0.5 A/g to 4 A/g, (e) cell capacitance, energy efficiency and coulombic efficiency values during 10,000 galvanostatic charge/discharge cycling up to 1.8 V and specific current 1.0 A/g, and (f) charge/discharge curves collected after every 1000 cycles, the arrow indicates the direction of increasing number of cycles.

indicate a stable asymmetric supercapacitor device that can withstand high rate cycling at 1.8 V. The galvanostatic charge/discharge curves after every 1000 cycles, superimposed in Fig. 5f, show a slight decrease of specific capacitance with cycle number. A capacitance loss during long-term cycling could originate from several factors, including the surface changes upon interaction with electrolyte to the accumulation of corrosion products at the electrode/current collector interface. The capacitance during long term cycling varies from 38 F/g to 37 F/g while the energy efficiency from 80% to 77.5% and coulombic efficiency from 93% to 90%, showing an overall excellent cycling performance.

Asymmetric supercapacitor with MnO_2/CNT|YP80F configuration was then tested at low temperatures. The supercapacitor performance was first investigated at 24°C and then the temperature was gradually reduced down to -40°C. Fig. 6 shows the electrochemical performance of MnO_2/CNT|YP80F supercapacitor at various temperatures. It can be seen in Fig. 6a,b that the capacitance drops by nearly 64% from 24°C to -40°C. Another noticeable aspect is the gradual increase of ohmic loss (indicated in CV at the charging point around 0.35 V in Fig. 6b and at the start of discharge in Fig. 6d) with decreasing temperature. In particular, at -40°C, the ohmic loss is ~0.45 V leading to low capacitance and also poor rate performance. CVs in Fig. 6b and galvanostatic charge/discharge curves in Fig. 6d collected at 50 mV/s and 1.0 A/g, respectively show that, while at room temperature there is negligible ohmic loss, the shape of the curves indicates quite resistive behavior at very low temperatures. Nevertheless, one can notice a much better capacitance retention at -30°C with almost symmetric charge/discharge curves and less resistive CVs.

3.4. Compraison of device performance parameters at different temperatures

Three performance key-parameters have been compared in Fig. 6, namely, capacitance (blue curves), energy efficiency (green curves) and coulombic efficiency (red curves) at various temperatures, were extracted from the galvanostatic charge/discharge at 0.5 A/g for the asymmetric MnO_2/CNT|YP80F supercapacitor polarized up to 1.8 V. Both the capacitance and energy efficiency are strongly influenced and show a decreasing trend with decreasing temperatures. A noticeable decrease of energy efficiency from 83% at 24°C to 58% at -40°C shows that the temperature has a drastic effect on the energy and power performance of the supercapacitor. At 24°C, on the other hand, by increasing the output voltage to 1.8 V the capacitance increases but the energy efficiency decreases (Fig. 7a). An increase in capacitance is commonly observed in hybrid supercapacitors containing carbon-based negative electrodes in aqueous electrolytes, which mainly originates from the reversible hydrogen adsorption/desorption in the carbon nanopores [11]. As discussed in Section 3.2, water is electrochemically reduced to produce hydrogen at low negative potentials in the carbon nanopores, and a part of this hydrogen is stored in the pores while other hydrogen participates in the chemical reaction with carbon to reversibly adsorb and desorb. These faradaic reactions at negative electrode that contribute to the overall cell capacitance are suppressed when shifting the temperature from 24°C to 0°C. Upon further decreasing the temperature, the capacitance and efficiency values display nearly a constant trend indicating the absence of faradaic reactions at the negative electrode and consequently no additional capacitance contribution. Another reason for the lower capacitance at low temperature is related to the low ionic conductivity of the electrolyte and hindered ionic movement in the carbon pores (indicated by higher ohmic drop as discussed in Fig. 6), and also has been explained in our previous studies [24].

Fig. 6h shows the galvanostatic charge/discharge curves up to 1.8 V at room temperature, -30°C, -40°C and at 60°C. One can also see a slightly higher capacitance at 60°C in Fig. 6i (red dots), which is mainly due to the increased faradaic contributions at higher temperatures related to the reduction of the aqueous electrolyte at the negative carbon electrode (i.e. H2 evolution and adsorption into the carbon pores).

Overall, MnO_2/CNT/YP80F asymmetric supercapacitor displays high capacitance, an improved performance due to the use of CNTs as electrode additive, which maintains increased electronic conductivity at low temperatures. The high solubility of choline nitrate in water makes

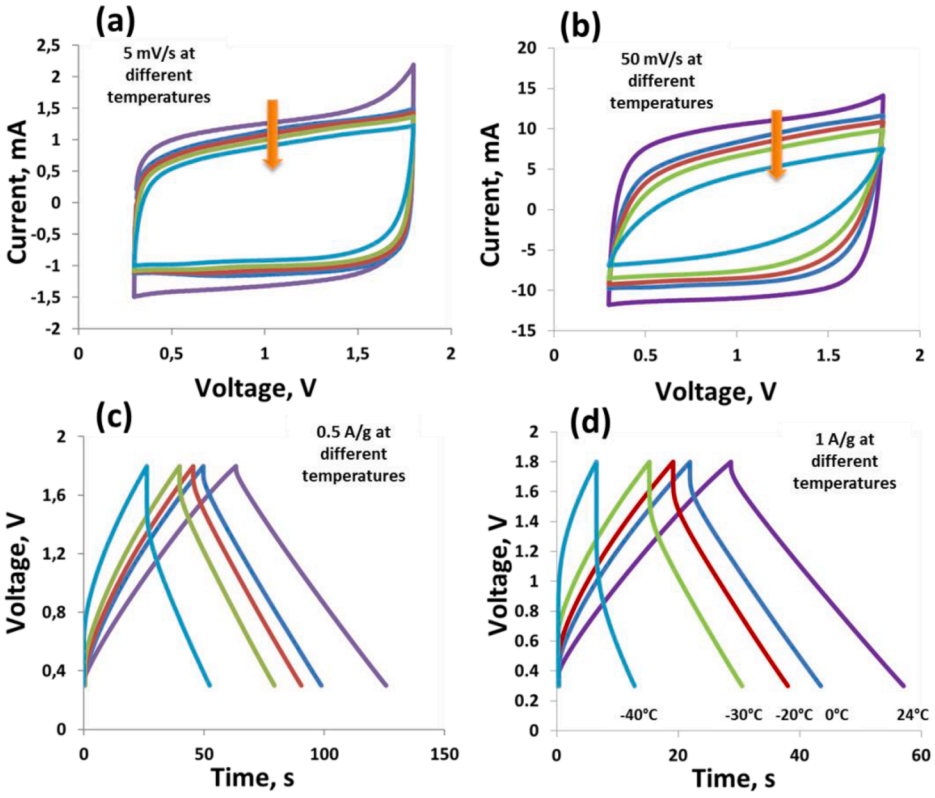

Fig. 6. Electrochemical behavior of MnO_2/CNT/YP80F supercapacitor in 5 mol/L $ChNO_3$ up to 1.8 V at 24°C, 0°C, -20°C, -30°C and -40°C, cyclic voltamogramms at different temperatures from room temperature to -40°C by using scan rates of (a) 5 mV/s and (b) 50 mV/s, galvanostatic charge/discharge curves at different temperatures from room temperature to -40°C by using specific currents (c) 0.5 A/g and (d) 1 A/g (the specific current is calculated per total active mass present in the two electrodes). The direction of arrows indicate the trend for decreasing discharge capacitance.

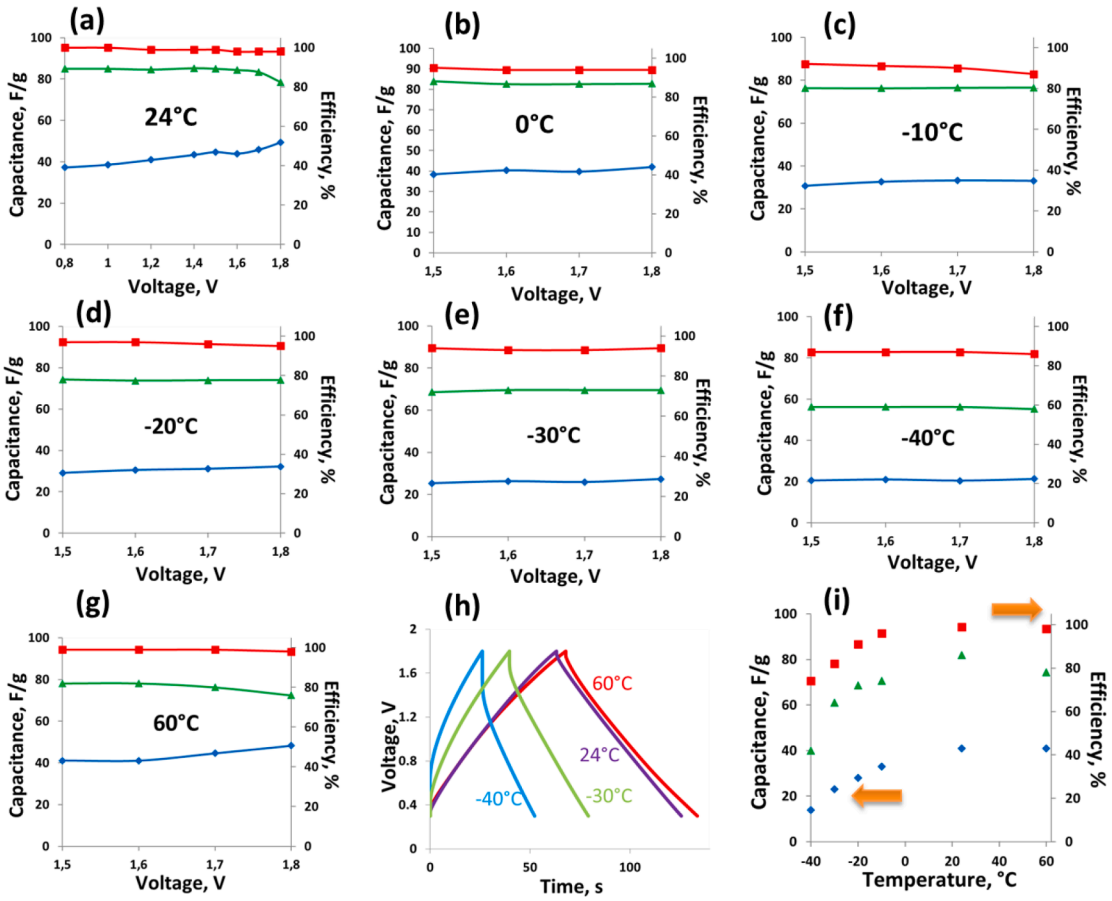

Fig. 7. Performance data (capacitance – blue curve, energy efficiency – green curve and coulombic efficiency – red curve) of MnO_2/CNT|YP80F supercapacitor in 5 mol/L $ChNO_3$ in voltage window from 1.5 V to 1.8 V at various temperatures (a) 24°C, (b) 0°C, (c) -10°C, (d) -20°C, (e) -30°C, (f) -40°C, (g) +60°C, (h) comparison of galvanostatic charge/discharge curves up to 1.8 V at 0.5 A/g and at different temperatures, and (i) capacitance, energy efficiency and coulombic efficiency values as function of temperature.

it a good choice as an electrolyte for asymmetric supercapacitor where the choline cation owing to its better dissociation, leads to improved electrodes charge/discharge behavior at low temperature.

4. Conclusion

The structure and morphology of MnO_2 can be controlled by adopting the hydrothermal process, where the presence of CNTs enhances the electron conductivity. The two-dimensional layered structure of MnO_2 improves the electrolyte accessibility and kinetics at the electrode/electrolyte interface. The $ChNO_3$-based aqueous electrolyte is advantageous due to its wide electrochemical stability window and excellent anti-freezing characteristics. Highly concentrated choline nitrate solution is suitable for low temperature and its performance is favored by the absence of any co-solvent that could disturb the local concentration in the carbon electrode nanopores. Therefore, the presence of a single solvent component facilitates the homogeneous adsorption of electrolyte into the porous carbon electrode as well accessibility onto the MnO_2/CNT-based electrode. Thanks to the high conductivity of aqueous choline nitrate at 5 mol/L and excellent low-temperature behavior, the MnO_2/CNT|YP80F supercapacitor demonstrates high cycle life and capacitance at 24°C and excellent energy efficiency and coulombic efficiency at -40°C. The presence of large choline cations with loose hydration shell enforces a charge storage mechanism of MnO_2 that is dictated by the anions adsorption. Owing to the reduced effect of ion-pairing in aqueous choline nitrate, the charge compensation is probably controlled by the counter ions (NO_3^- ions) – simply the large choline cation easily liberates the counter ion.

CRediT authorship contribution statement

Sandra Schrade: Investigation, Methodology, Formal analysis, Writing – original draft. **Zijian Zhao:** Conceptualization, Investigation, Formal analysis, Software, Writing – original draft. **Zhazira Supiyeva:** Data curation, Methodology. **Xinman Chen:** Formal analysis, Validation, Methodology. **Sonia Dsoke:** Conceptualization, Methodology, Supervision, Writing – review & editing, Project administration. **Qamar Abbas:** Conceptualization, Supervision, Investigation, Validation, Methodology, Writing – review & editing.

Declaration of Competing Interest

The authors declare that they have no known competing financial interests or personal relationships that could have appeared to influence the work reported in this paper.

Acknowledgments

Q.A thanks The Austrian Research Promotion Agency (FFG) Austria for providing funds for the project number 39966764. S.D., Z.Z. and S.S. would like to thank the financial support from the German Federal Ministry of Education and Research (BMBF) Germany under the Grant FKZ 01DH20025 (project SuBLiME). This work contributes to the research performed at CELEST (Center for Electrochemical Energy Storage Ulm-Karlsruhe).

References

[1] A. Burke, Ultracapacitors: why, how, and where is the technology, J. Power Sources 91 (2000) 37.

[2] A. Janes, E. Lust, Use of organic esters as co-solvents for electrical double layer capacitors with low temperature performance, J. Electroanal. Chem. 588 (2006) 285.

[3] G. Wang, L. Zhang, J. Zhang, A review of electrode materials for electrochemical supercapacitors, Chem. Soc. Rev. 41 (2012) 797.

[4] B. Kim, S. Sy, A. Yu, J. Zhang, Electrochemical Supercapacitors for Energy Storage and Conversion. Handbook of Clean Energy Systems, John Wiley & Sons, 2015, pp. 1–25, https://doi.org/10.1002/9781118991978.hces112.

[5] Q. Abbas, B. Gollas, V. Presser, Reduced Faradaic Contributions and Fast Charging of Nanoporous Carbon Electrodes in a Concentrated Sodium Nitrate Aqueous Electrolyte for Supercapacitors, Energy Technol. 7 (2019), 1900430.

[6] D. Reber, R.S. Kühnel, C. Battaglia, High-voltage aqueous supercapacitors based on NaTFSI, Sustain. Energy Fuels 1 (2017) 2155.

[7] M.S. Hong, S.H. Lee, S.W. Kim, Use of KCl Aqueous Electrolyte for 2 V Manganese Oxide/Activated Carbon Hybrid Capacitor, Electrochem. Solid-State Lett. 5 (2002) A227.

[8] C.C. Hu, T.W. Tsou, Capacitive and textural characteristics of hydrous manganese oxide prepared by anodic deposition, Electrochim. Acta 47 (2002) 3523.

[9] T. Brousse, P.L. Taberna, O. Crosnier, R. Dugas, P. Guillemet, Y. Scudeller, Y. Zhou, F. Favier, D. Bélanger, P. Simon, Long-term cycling behavior of asymmetric activated carbon/MnO2 aqueous electrochemical supercapacitor, J. Power Sources 173 (2007) 633.

[10] L. Demarconnay, E. Raymundo-Piñero, F. Béguin, Adjustment of electrodes potential window in an asymmetric carbon/MnO_2 supercapacitor, J. Power Sources 196 (2011) 580.

[11] S.E. Chun, J. Whitacre, Investigating the role of electrolyte acidity on hydrogen uptake in mesoporous activated carbons, J. Power Sources 242 (2013) 137.

[12] Y. Hou, Y. Cheng, T. Hobson, J. Liu, Design and Synthesis of Hierarchical MnO_2 Nanospheres/Carbon Nanotubes/Conducting Polymer Ternary Composite for High Performance Electrochemical Electrodes, Nano Lett. 10 (2010) 2727.

[13] J.W. Wang, Y. Chen, B-Z. Chen, Synthesis and control of high-performance MnO_2/carbon nanotubes nanocomposites for supercapacitors, J. Alloy. Compd. 688 (2016) 184.

[14] Z. Lei, F. Shi, L. Lu, Incorporation of MnO_2-Coated Carbon Nanotubes between Graphene Sheets as Supercapacitor Electrode, ACS Appl. Mater. Interfaces 4 (2012) 1058.

[15] M. Toupin, T. Brousse, D. Belanger, Charge Storage Mechanism of MnO_2 Electrode Used in Aqueous Electrochemical Capacitor, Chem. Mater. 16 (2004) 3184.

[16] P. Simon, Y. Gogotsi, Materials for electrochemical capacitors, Nat. Mater. 7 (2008) 845.

[17] C. Costentin, J.M. Saveant, Energy storage: pseudocapacitance in prospect, Chem. Sci. 10 (2019) 5656.

[18] J.K. Chang, M.T. Lee, W.T. Tsai, M.J. Deng, H.F. Cheng, I.W. Sun, Pseudocapacitive Mechanism of Manganese Oxide in 1-Ethyl-3-methylimidazolium Thiocyanate Ionic Liquid Electrolyte Studied Using X-ray Photoelectron Spectroscopy, Langmuir 25 (2009) 11955.

[19] Q. Abbas, F. Beguin, High voltage AC/AC electrochemical capacitor operating at low temperature in salt aqueous electrolyte, J. Power Sources 318 (2016) 235.

[20] Q. Abbas, P. Nürnberg, R. Ricco, F. Carraro, B. Gollas, M. Schönhoff, Less Water, Naked Choline, and Solid Iodine for Superior Ecofriendly Hybrid Energy Storage, Adv. Energy Sustain. Res. 2 (2021), 2100115.

[21] Q. Abbas, L. Binder, Synthesis and Characterization of Choline Chloride Based Binary Mixtures, ECS Trans. 33 (2010) 49.

[22] E. Smith, A. Abbott, K. Ryder, Deep Eutectic Solvents (DESs) and Their Applications, Chem. Rev. 114 (2014) 11060.

[23] L. Vieira, R. Schennach, B. Gollas, In situ PM-IRRAS of a glassy carbon electrode/deep eutectic solvent interface, Phys. Chem. Chem. Phys. 17 (2015) 12870.

[24] Q. Abbas, F. Beguin, Sustainable Carbon/Carbon Supercapacitors Operating Down to −40 °C in Aqueous Electrolyte Made with Cholinium Salt, ChemSusChem 11 (2018) 975.

[25] H. Xia, Y. Wang, J. Lin, L. Lu, Hydrothermal synthesis of MnO_2/CNT nanocomposite with a CNT core/porous MnO_2 sheath hierarchy architecture for supercapacitors, Nanoscale Res. Lett. 7 (2012) 1.

[26] O. Curnow, D. MacFarlane, K. Walst, Fluoride Ionic Liquids in Salts of Ethylmethylimidazolium and Substituted Cyclopropenium Cation Families, Front. Chem. 6 (2018) 603.

[27] J. Luo, H. Zhu, H. Fan, J. Liang, H. Shi, G. Rao, J. Li, Z. Du, Z. Shen, Synthesis of Single-Crystal Tetragonal α-MnO_2 Nanotubes, J. Phys. Chem. C 112 (2008) 12594.

[28] A. Shalaby, et al., Structural analysis of reduced graphene oxide by transmission electron microscopy, Bulg. Chem. Commun. 47 (2015) 291.

[29] L. Suo, O. Borodin, T. Gao, M. Olguin, J. Ho, X. Fan, C. Luo, C. Wang, K. Xu, "Water-in-salt" electrolyte enables high-voltage aqueous lithium-ion chemistries, Science 350 (2015) 938.

[30] K. Reddy, H. Jeong, Y. Lee, A. Raghu, Synthesis of MWCNTs-core/thiophene polymer-sheath composite nanocables by a cationic surfactant-assisted chemical oxidative polymerization and their structural properties, J. Polym. Sci. Polym. Chem. 48 (2010) 1477.